Electronic Supplementary Material (ESI) for Dalton Transactions.

Aerobic Oxygenation Catalyzed by First Row Transition Metal Complexes Coordinated by Tetradentate Mono-Carbon Bridged Bis-Phenanthroline Ligands: Intra- versus Intermolecular Carbon-Hydrogen Bond Activation

Kaiji Shen, Yael Diskin-Posner, Linda J. W. Shimon, Gregory Leitus, Raanan Carmieli, and Ronny Neumann

Electronic Supporting Information

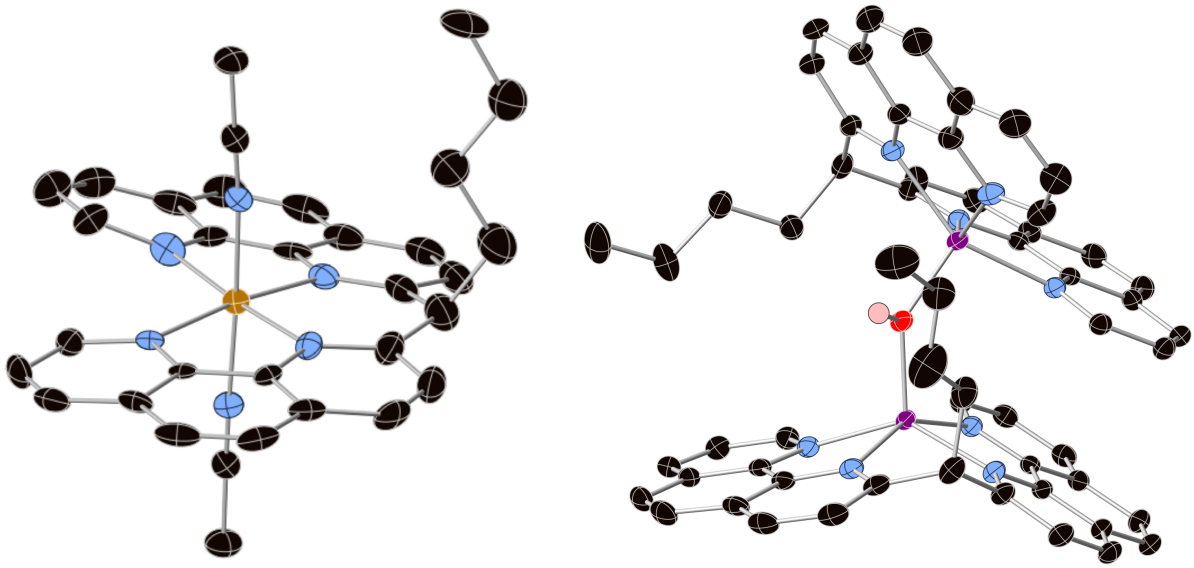

Figure S1. Thermal Ellipsoid Structure of Fe(II)-**L3** (left) and Zn(II)-**L3** (right) at 50% probability. The PF_6 anions and H atoms (except for the hydroxy moiety) are not shown, Fe-brown, Zn-purple, O-red, N-blue, C-black, H-pink.

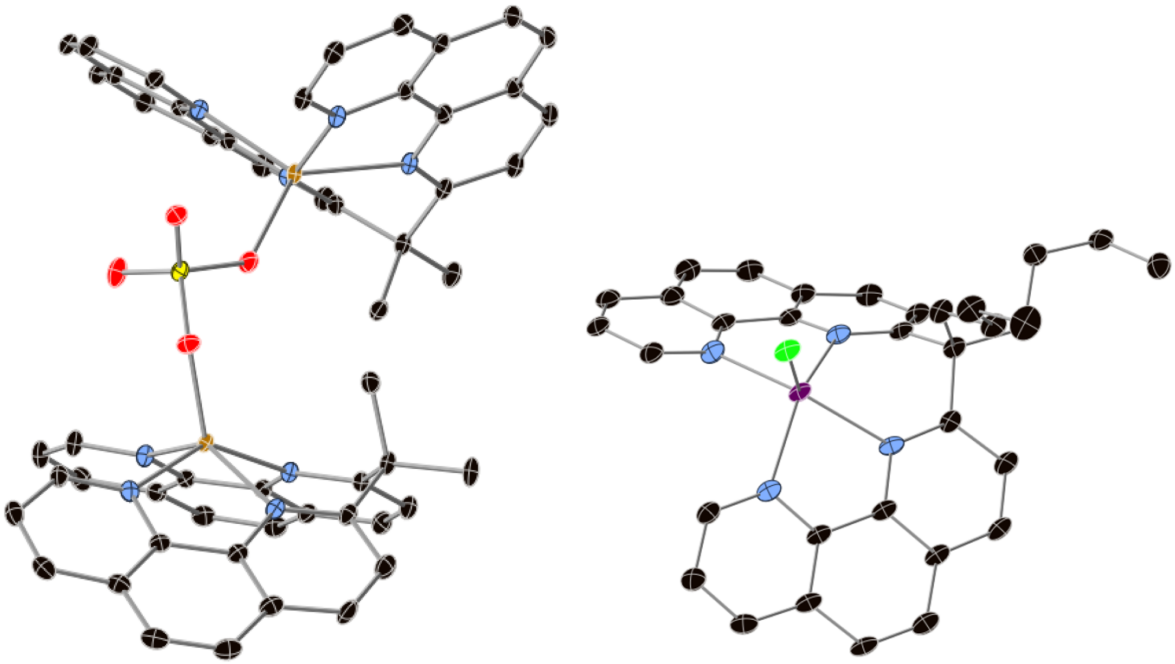

Figure S2. Thermal Ellipsoid Structure of Fe(II)-**L4** (left) and Zn(II)-**L4** (right) at 50% probability. The PF_6 anions and H atoms are not shown. Fe-brown, Zn-purple, O-red, S-yellow, N-blue, C-black.

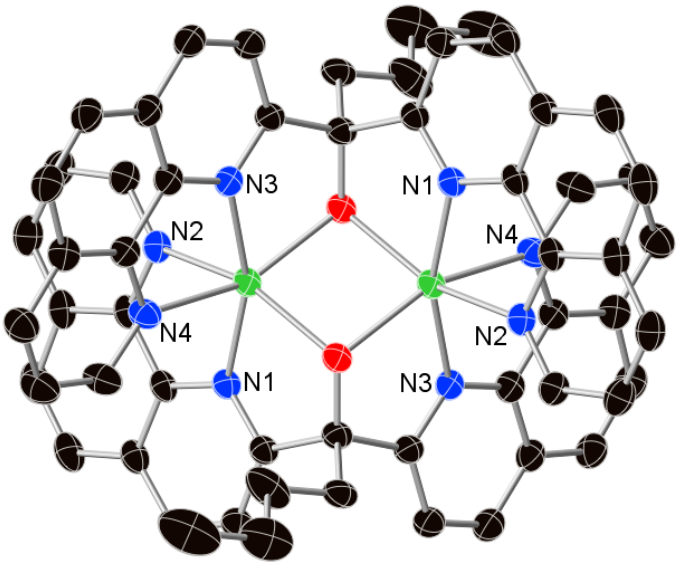

Figure S3. Thermal Ellipsoid Structure of Complex **11** at 50% probability. The PF_6 anions and H atoms are not shown, Co-green, N-blue, C-black, O-red.

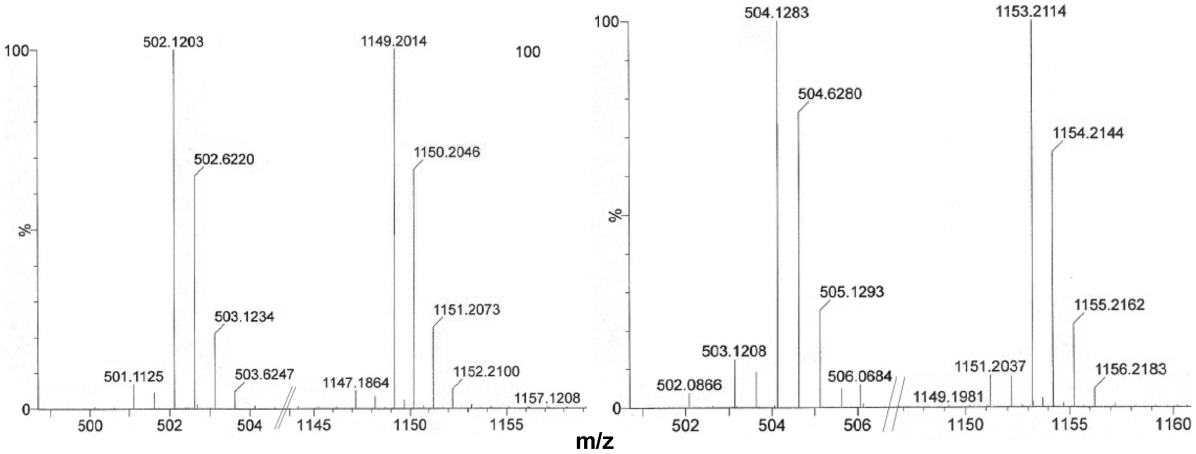

Figure S4. HR ESI-MS of Complex **11** formed from $^{16}O_2$ (left) and $^{18}O_2$ (right)

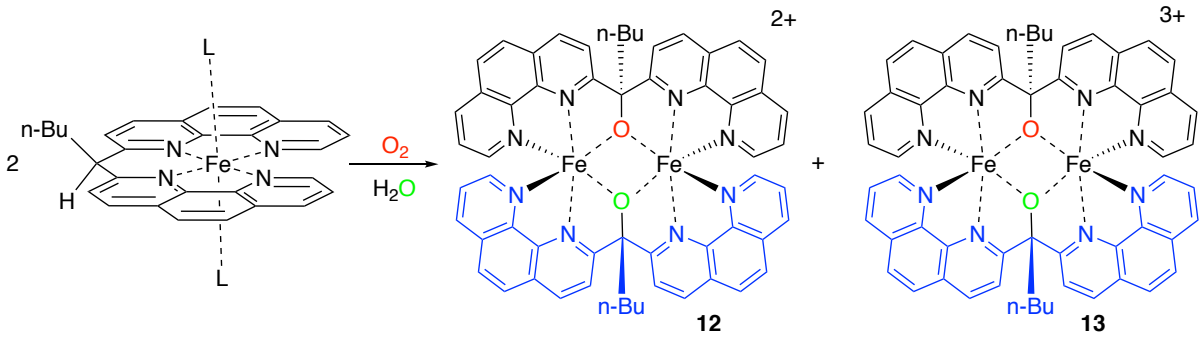

Scheme S1. Reaction of Fe(II)-**L3** with O_2

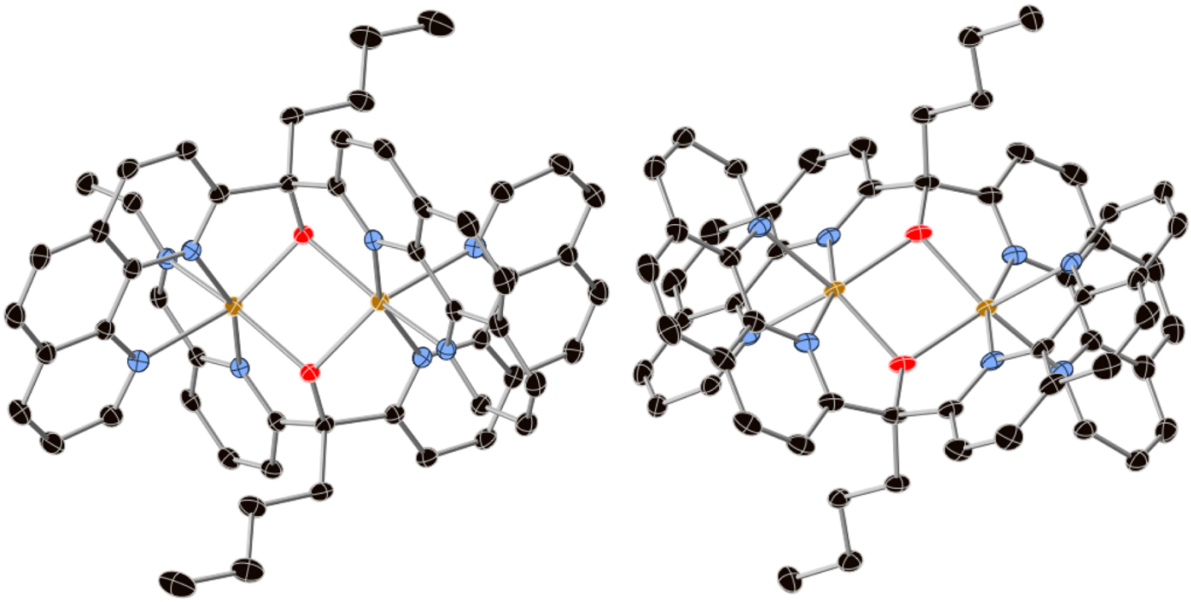

Figure S5. Thermal Ellipsoid Structure of Complex **12** (left) and **13** (right) at 50% probability. The PF_6 anions and H atoms are not shown, Fe-brown, N-blue, C-black, O-red.

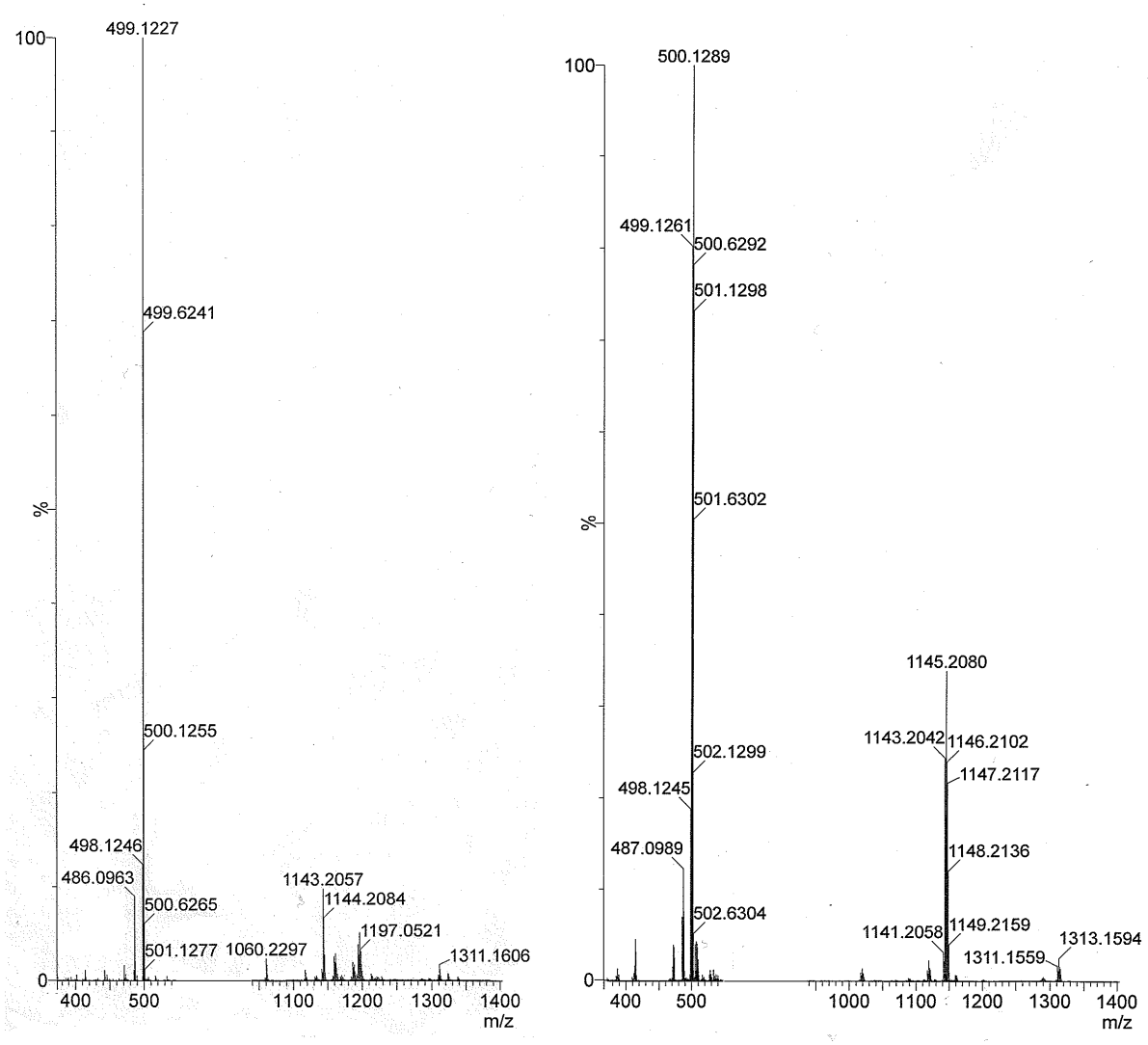

Figure S6. HR ESI-MS of Complex **12** formed from $^{16}O_2$ (left) and $^{18}O_2$ (right) where z = 1 or 2

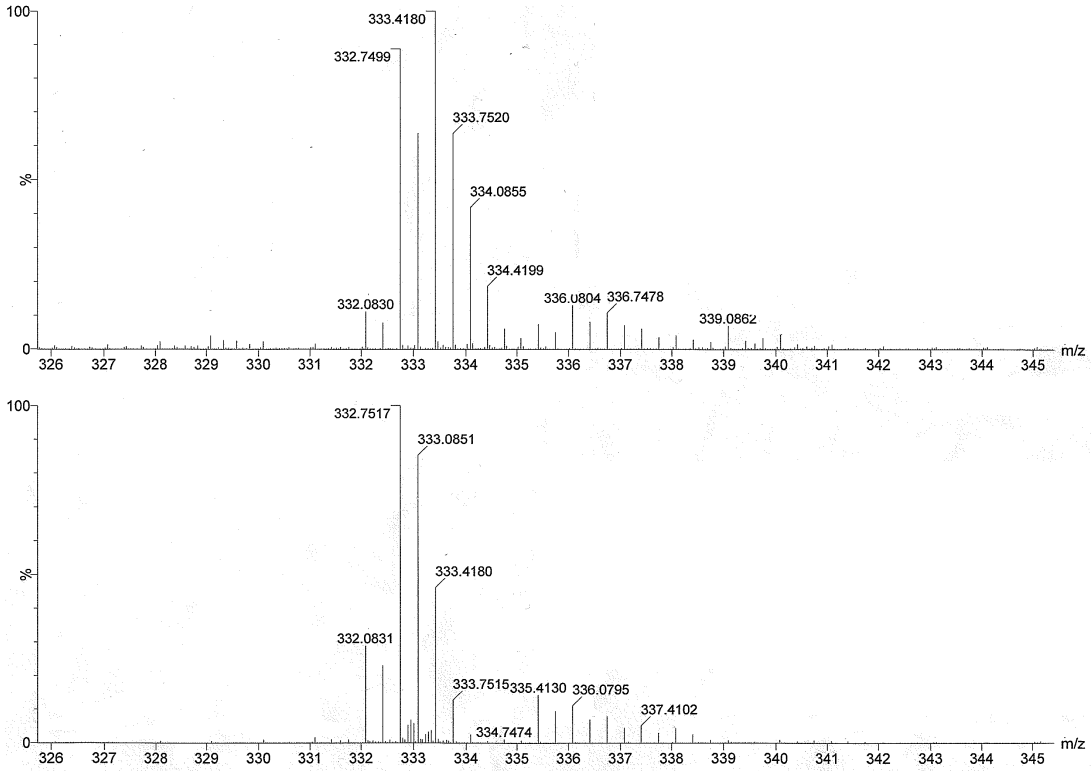

Figure S7. HR ESI-MS of Complex **13** where z = 3 from $^{16}O_2$ (bottom) and from $^{18}O_2$ (top)

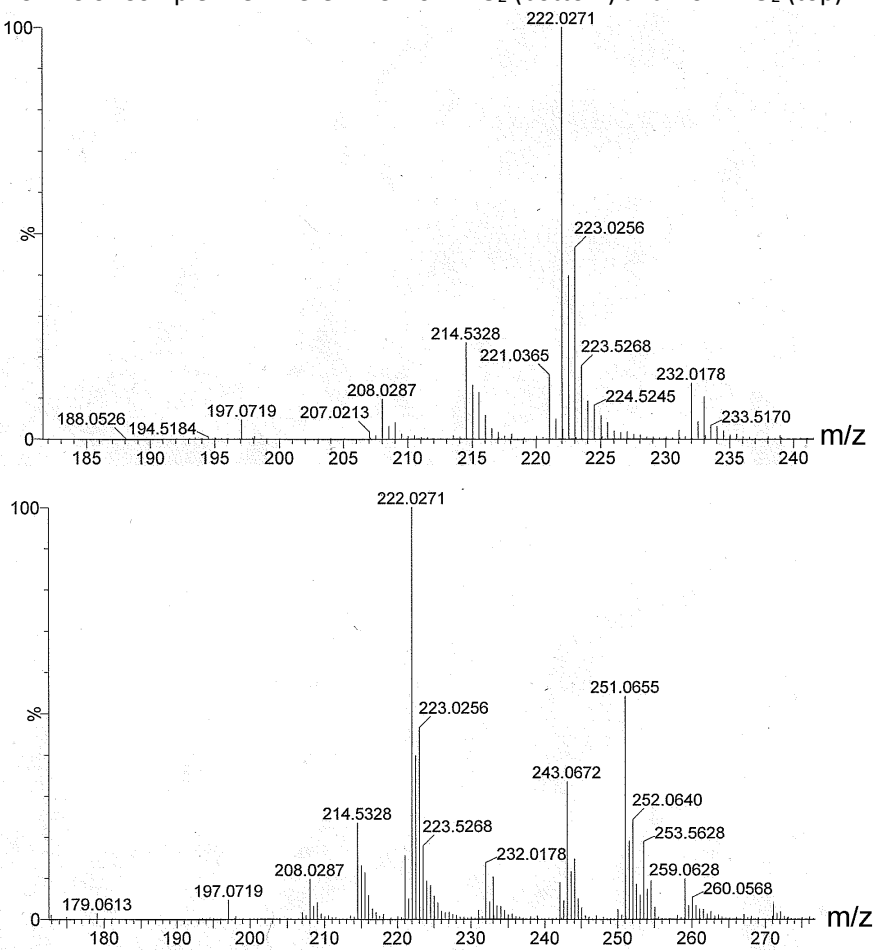

Figure S8. HR ESI-MS of Complex **14** (top) and **15** (bottom) where z = 2. Compound **15** is not pure and contains Compound **14**.

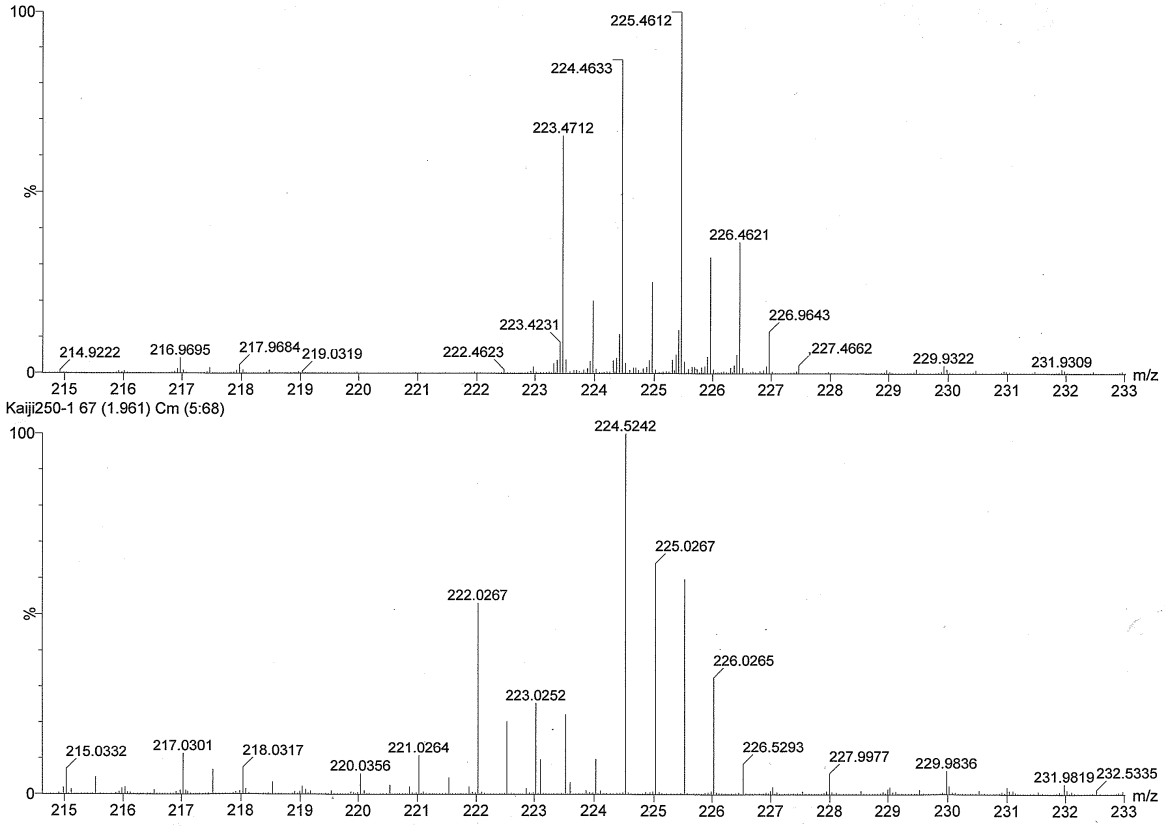

Figure S9. HR ESI-MS of Complex **16** where z = 2 from $^{16}O_2$ (bottom) and from $^{18}O_2$ (top)

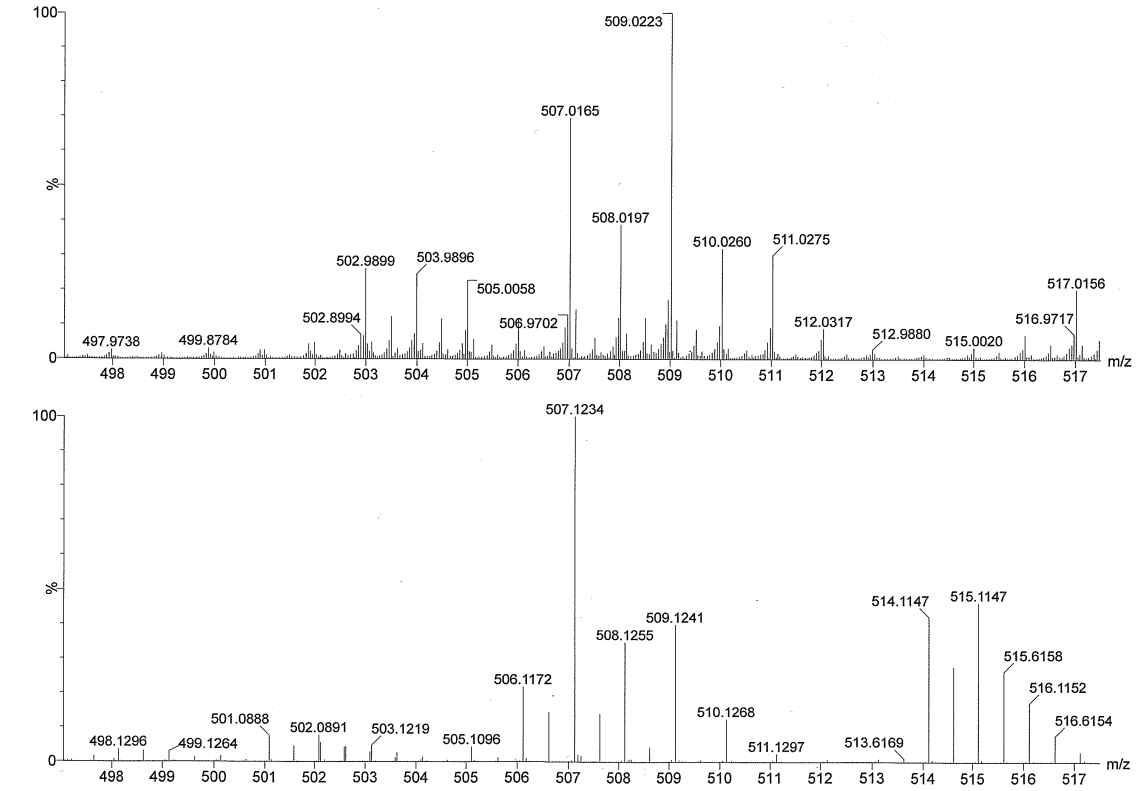

Figure S10. HR ESI-MS of Complex **17** where z = 2 from $^{16}O_2$ (bottom) and from $^{18}O_2$ (top)

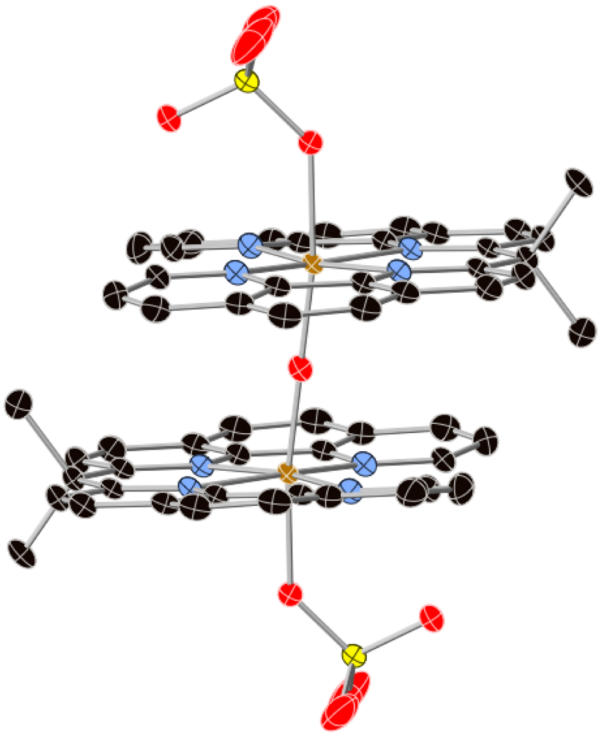

Figure S11. Thermal Ellipsoid Structure of the Fe(III)-μ-O-Fe(III) Compound Formed During Intermolecular Oxidation of Cyclohexene. 50% probability. The PF_6 anions and H atoms are not shown, Fe-brown, N-blue, C-black, O-red, S-yellow.

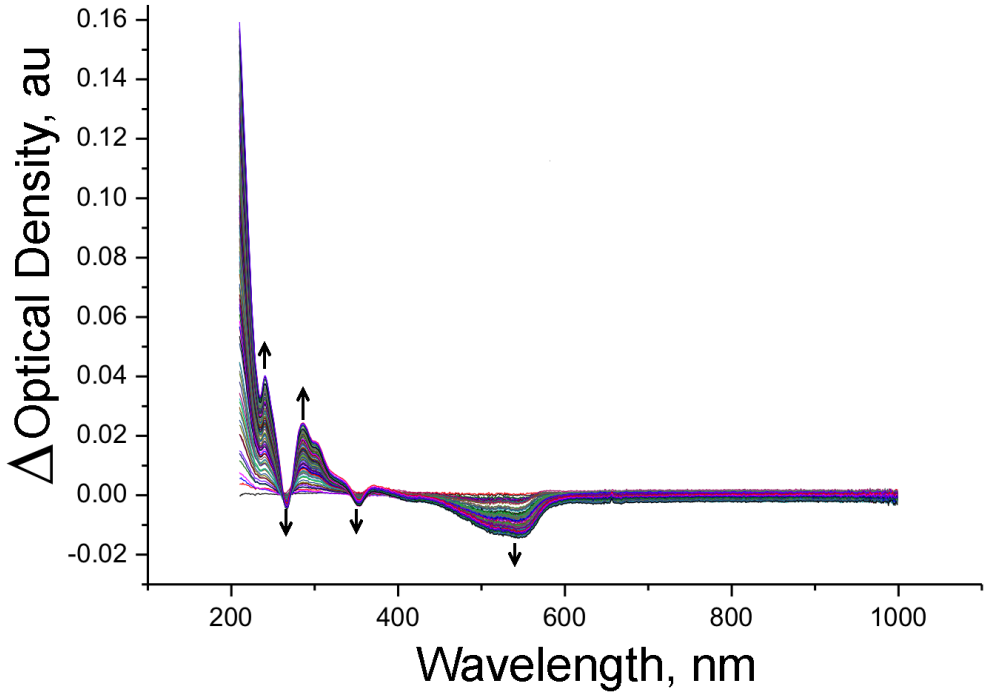

Figure S12. UV-vis spectra shown as difference spectra ($t_x - t_0$) for clarity at RT of the reaction of 0.01 mM Co(II)-**L3** in MeOH in the presence of O_2 (1 bar air). Time 0 – 250 s. Isosbestic points at 261, 273, 341 and 360 nm.

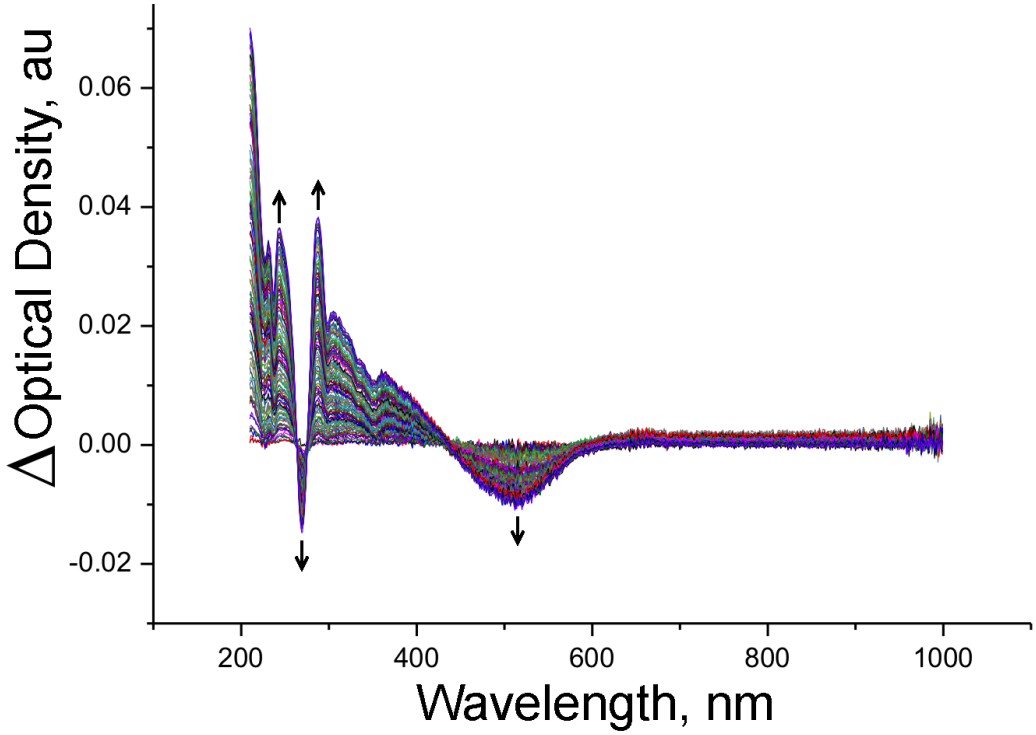

Figure S13. UV-vis spectra shown as difference spectra ($t_x - t_0$) for clarity at RT of the reaction of 0.01 mM Fe(II)-**L3** in MeOH in the presence of O_2 (1 bar air). Time 0 – 90 s. Isosbestic points at 263, 275, 435 nm.

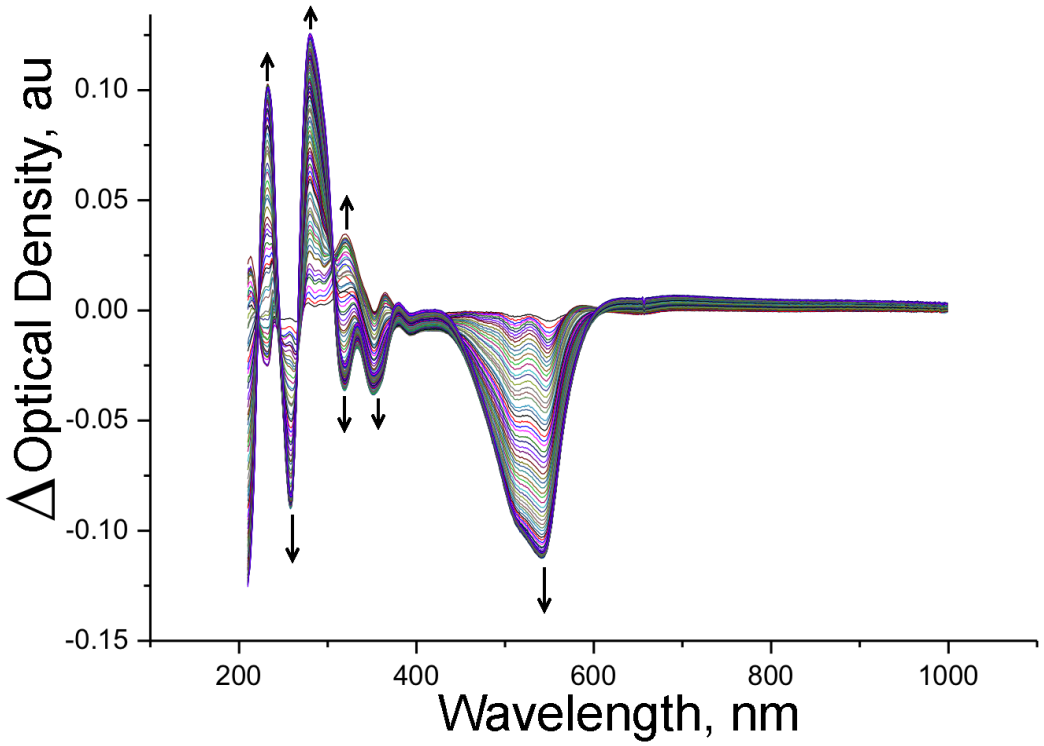

Figure S14. UV-vis spectra shown as difference spectra ($t_x - t_0$) for clarity at RT of the reaction of 0.01 mM Ni(II)-**L3** in 1:1 MeOH/MeCN in the presence of O_2 (1 bar air). Time 0 – 600 s. Isosbestic points at 245, 266, 305, 375 nm.

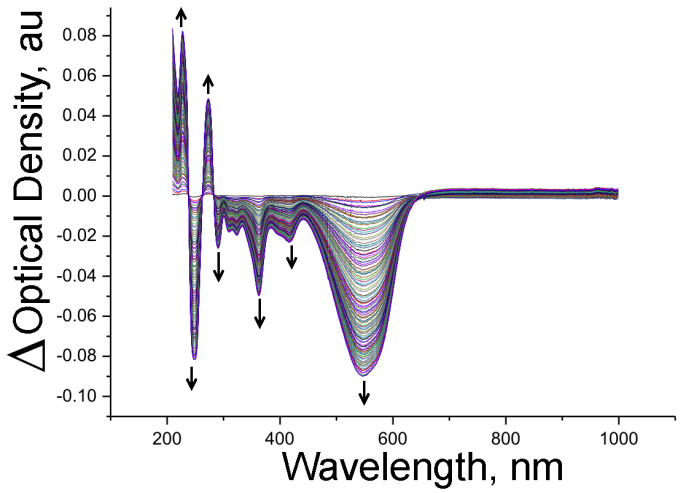

Figure S15. UV-vis spectra shown as difference spectra ($t_x - t_0$) for clarity at RT of the reaction of 0.01 mM Cu(II)-**L3** in 1:1 MeOH/MeCN in the presence of O_2 (1 bar air). Time 0 – 100 s. Isosbestic points at 240, 263, 282 nm.

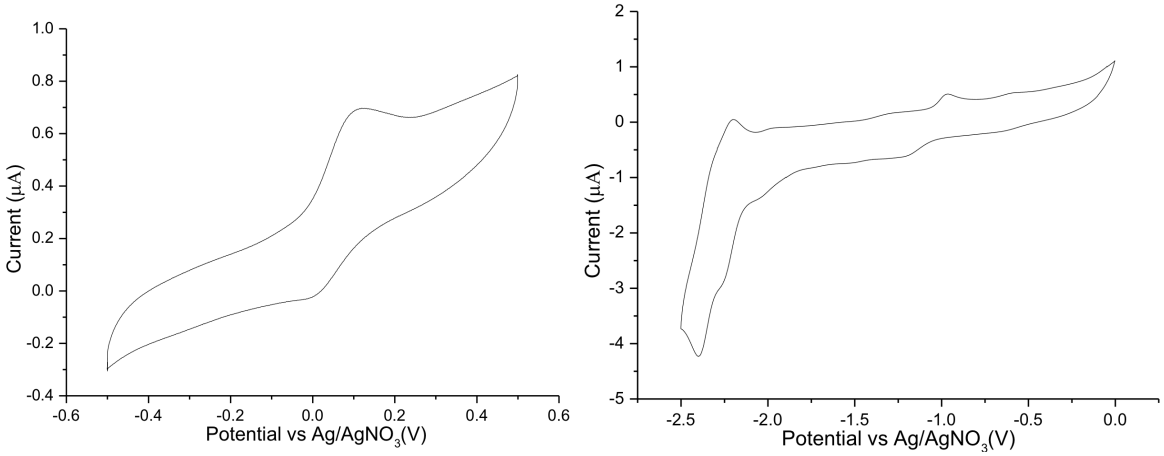

Figure S16. Cyclic voltammogram of 0.5 mM **L3** in DMF with 0.1 M Bu_4NPF_6 as electrolyte. Oxidation (left) at 0.1 V; Reduction (right) at -1.1 V. Working electrode –glassy carbon; Counter electrode – Pt; Reference electrode – $Ag/AgNO_3$; scan rate –50 mV/sec.

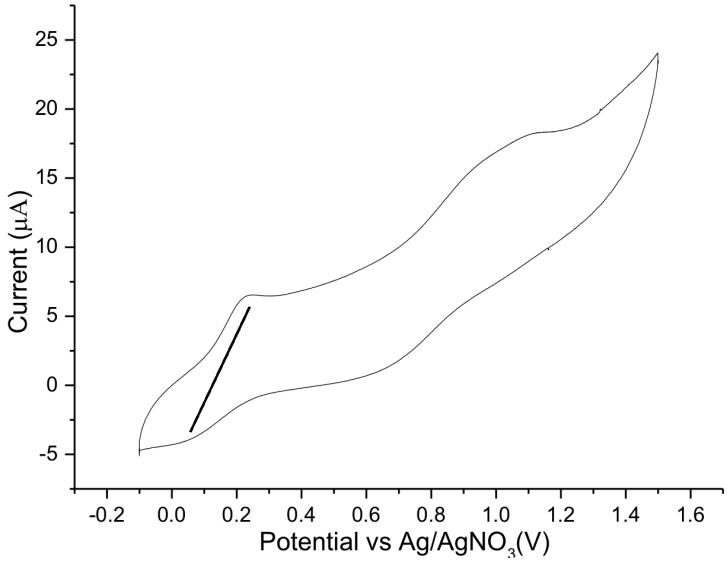

Figure S17. Cyclic voltammogram (oxidation) of 0.6 mM Ni(II)-**L3** in MeCN under N_2 in an "oxygen free glovebox" with 0.1 M Bu_4NPF_6 as electrolyte. Working electrode –glassy carbon; Counter electrode – Pt; Reference electrode – $Ag/AgNO_3$; scan rate –50 mV/sec.

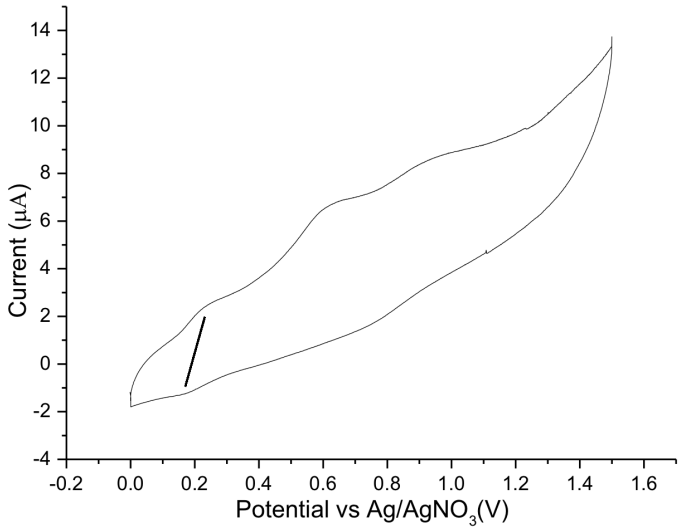

Figure S18. Cyclic voltammogram (oxidation) of 0.6 mM Cu(II)-**L3** in MeCN under N_2 in an "oxygen free" glovebox with 0.1 M Bu_4NPF_6 as electrolyte. Working electrode –glassy carbon; Counter electrode – Pt; Reference electrode – $Ag/AgNO_3$; scan rate –50 mV/sec.

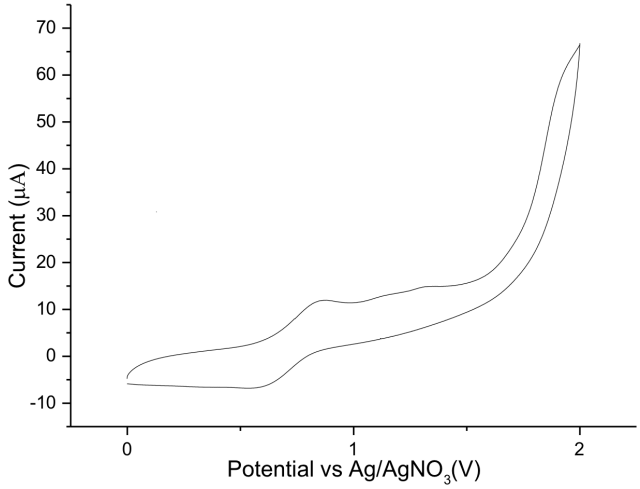

Figure S19. Cyclic voltammogram (oxidation) of 0.4 mM Co(II)-**L3** in MeCN under N_2 in an "oxygen free" glovebox with 0.1 M Bu_4NPF_6 as electrolyte. Working electrode –glassy carbon; Counter electrode – Pt; Reference electrode – $Ag/AgNO_3$; scan rate –50 mV/sec.

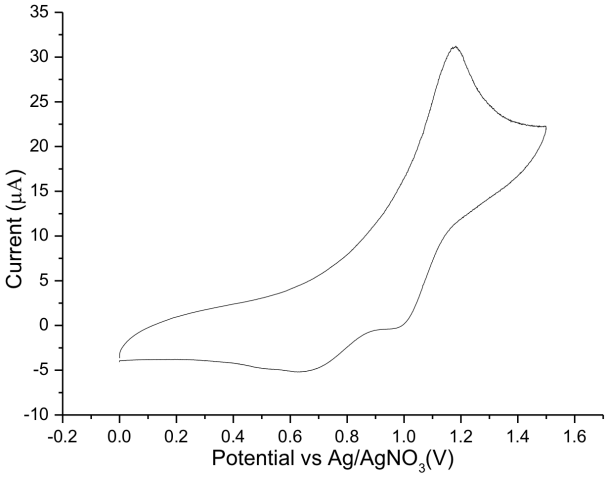

Figure S20. Cyclic voltammogram (oxidation) of 0.6 mM Fe(II)-**L3** in MeCN under N_2 in an "oxygen free" glovebox with 0.1 M Bu_4NPF_6 as electrolyte. Working electrode –glassy carbon; Counter electrode – Pt; Reference electrode – $Ag/AgNO_3$; scan rate –50 mV/sec.

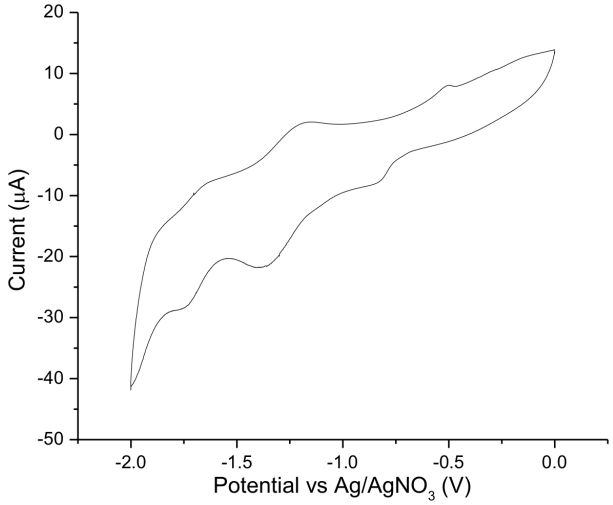

Figure S21. Cyclic voltammogram (reduction) of 0.6 mM Ni(II)-**L3** in MeCN under N_2 in an "oxygen free glovebox" with 0.1 M Bu_4NPF_6 as electrolyte. Working electrode –glassy carbon; Counter electrode – Pt; Reference electrode – $Ag/AgNO_3$; scan rate –50 mV/sec.

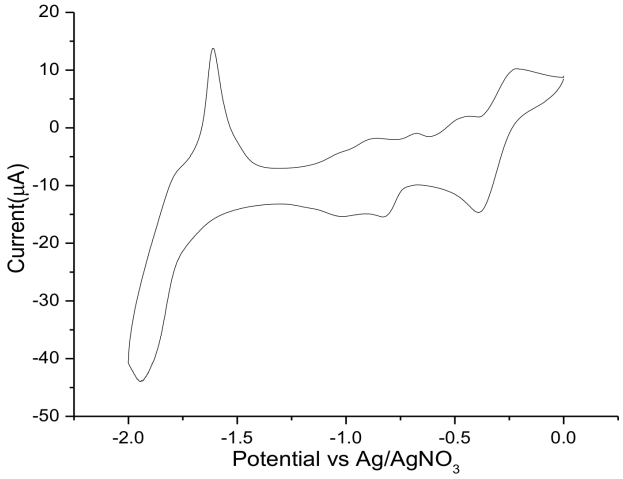

Figure S22. Cyclic voltammogram (reduction) of 0.6 mM Cu(II)-**L3** in MeCN under N_2 in an "oxygen free glovebox" with 0.1 M Bu_4NPF_6 as electrolyte. Working electrode –glassy carbon; Counter electrode – Pt; Reference electrode – $Ag/AgNO_3$; scan rate –50 mV/sec.

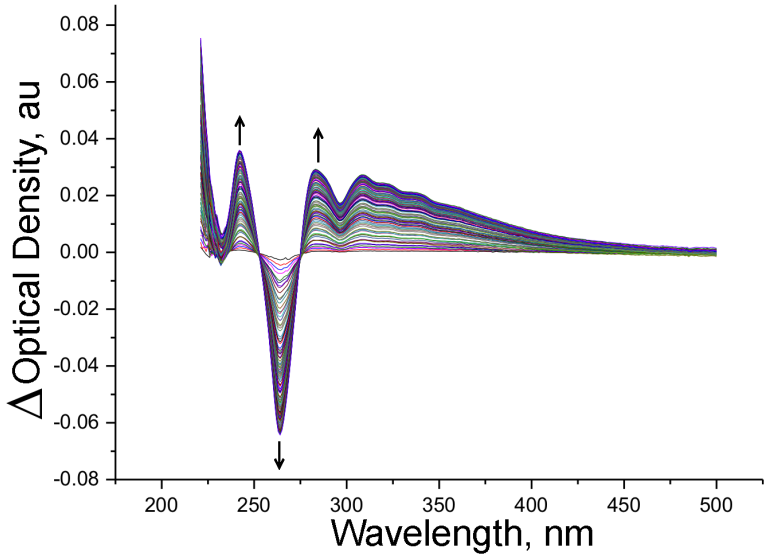

Figure S23. UV-vis spectra shown as difference spectra ($t_x - t_0$) for clarity at RT of the reaction of 0.1 mM Co(II)-**L4** in MeOH in the presence of 1 mM cyclohexene and O_2 (1 bar air). Isosbestic points at 253, 277 nm.

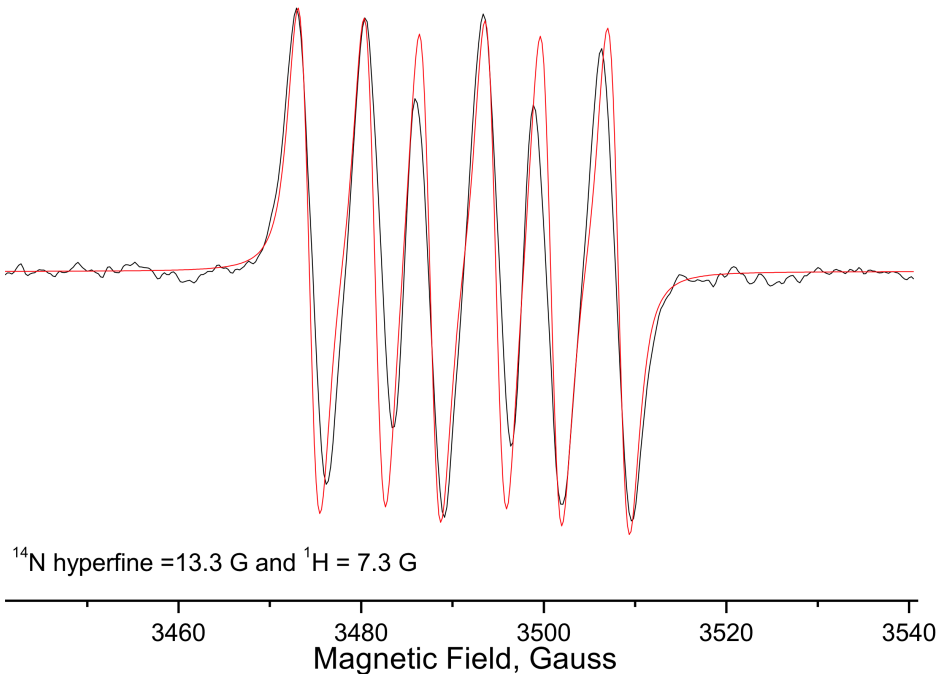

Figure S24. X-band EPR spectrum at room temperature of 5 mM Ni(II)-**L4** in the presence of 0.1 M cyclohexene and 10 mM BMPO under 1 bar O_2. Black – measured spectrum; red – simulated spectrum.

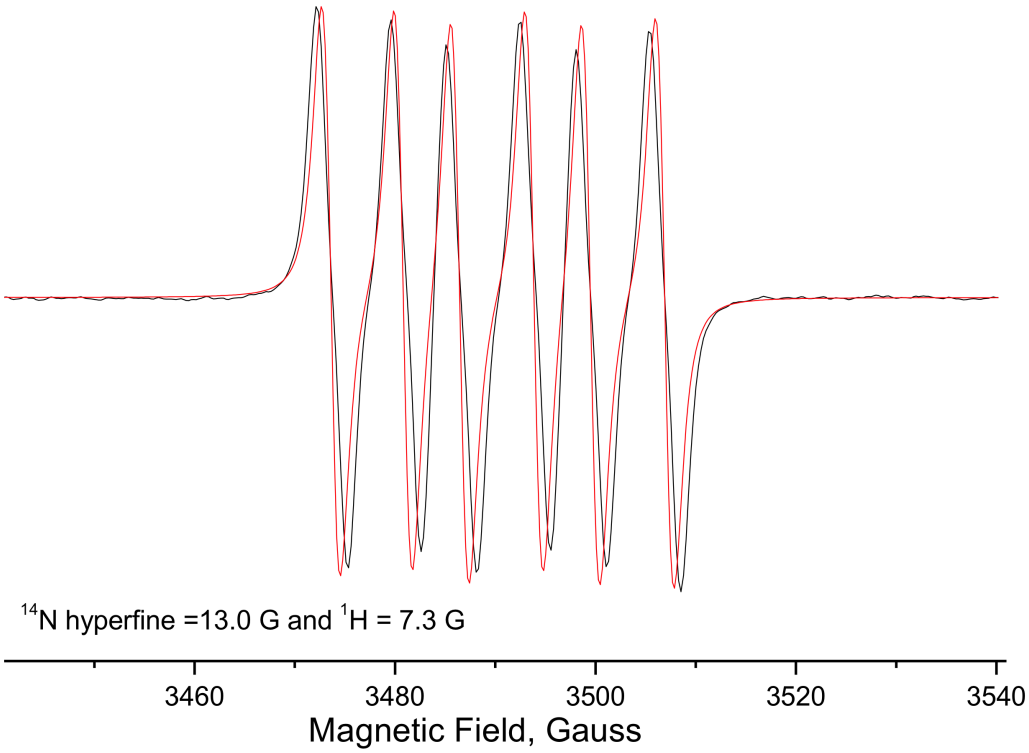

Figure S25. X-band EPR spectrum at room temperature of 5 mM Cu(II)-**L4** in the presence of 0.1 M cyclohexene and 10 mM BMPO under 1 bar O_2. Black – measured spectrum; red – simulated spectrum.

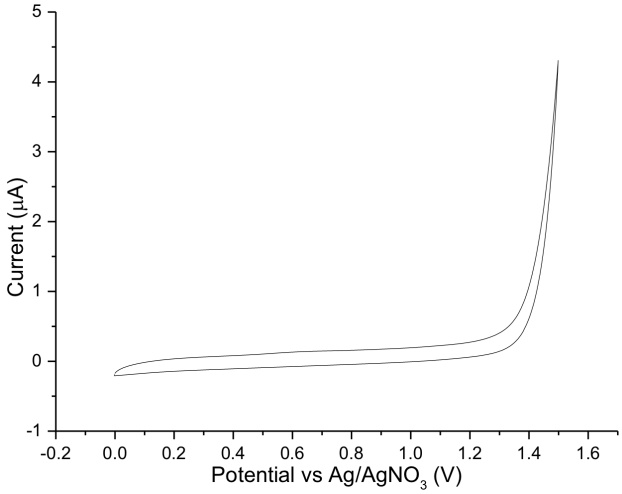

Figure S26. Cyclic voltammogram of 10 mM cyclohexene in acetonitrile with 0.1 M Bu_4NPF_6 as electrolyte under Ar. Working electrode –glassy carbon; Counter electrode – Pt; Reference electrode – $Ag/AgNO_3$; scan rate –50 mV/sec.

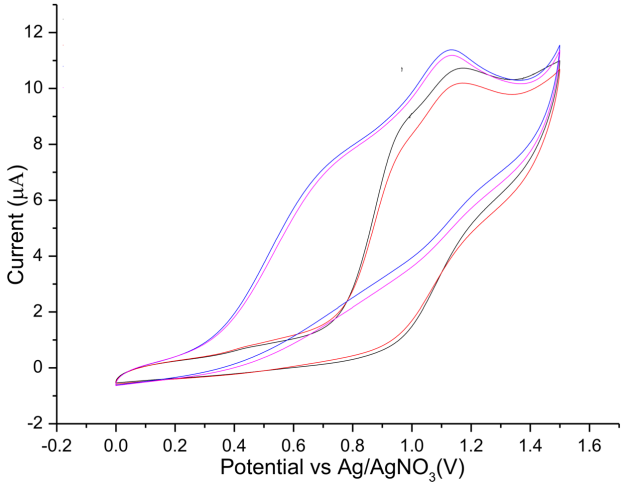

Figure S27. Cyclic voltammogram of 0.4 mM Cu(II)-**L4** in acetonitrile with 0.1 M Bu_4NPF_6 as electrolyte. Working electrode –glassy carbon; Counter electrode – Pt; Reference electrode – $Ag/AgNO_3$; scan rate –50 mV/sec. Black –1 bar Ar; Red - 1 bar air; Blue - 10 mM cyclohexene, 1 bar Ar; Magenta - 10 mM cyclohexene, 1 bar air.

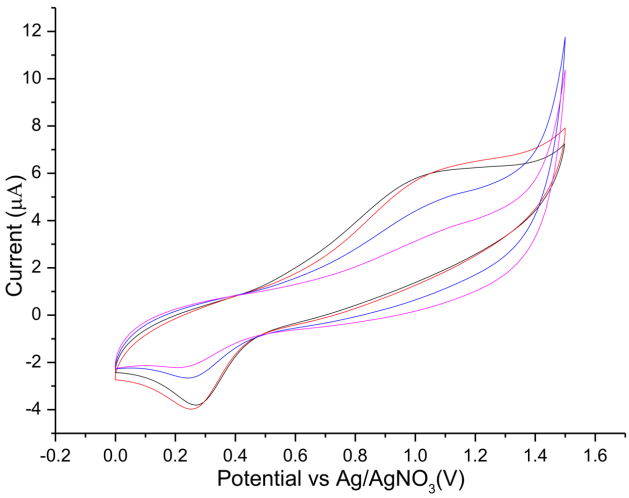

Figure S28. Cyclic voltammogram of 0.4 mM Co(II)-**L4** in acetonitrile with 0.1 M Bu_4NPF_6 as electrolyte. Working electrode –glassy carbon; Counter electrode – Pt; Reference electrode – $Ag/AgNO_3$; scan rate –50 mV/sec. Black –1 bar Ar; Red - 1 bar air; Blue - 10 mM cyclohexene, 1 bar Ar; Magenta - 10 mM cyclohexene, 1 bar air.

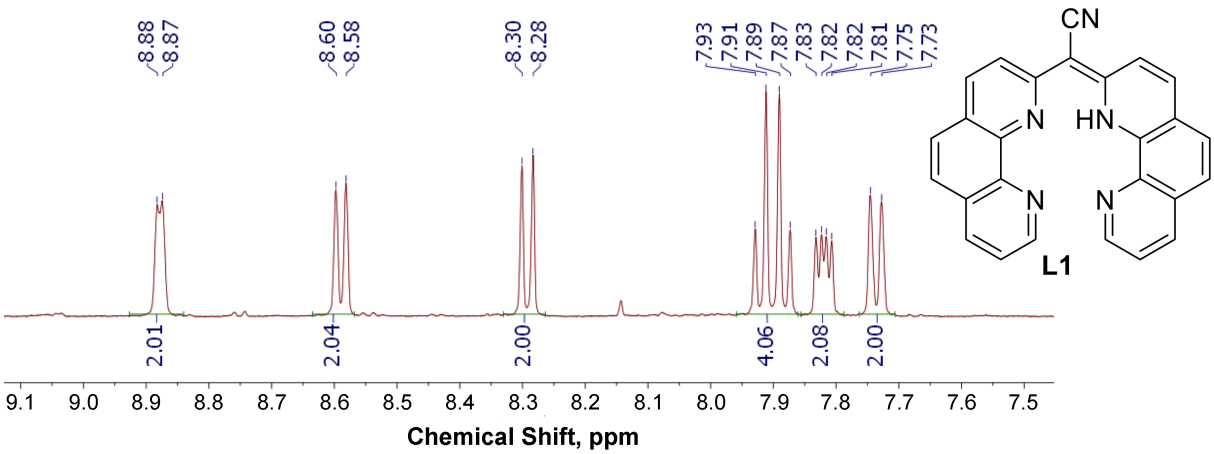

Figure S29.[1]H NMR of **L1**. Note that this spectrum was measured at 373.2 K in order to obtain a good resolution of the peaks. At this temperature the N-H proton undergoes fast exchange and is not observed. It can be observed at RT as a singlet at 16.14 ppm.

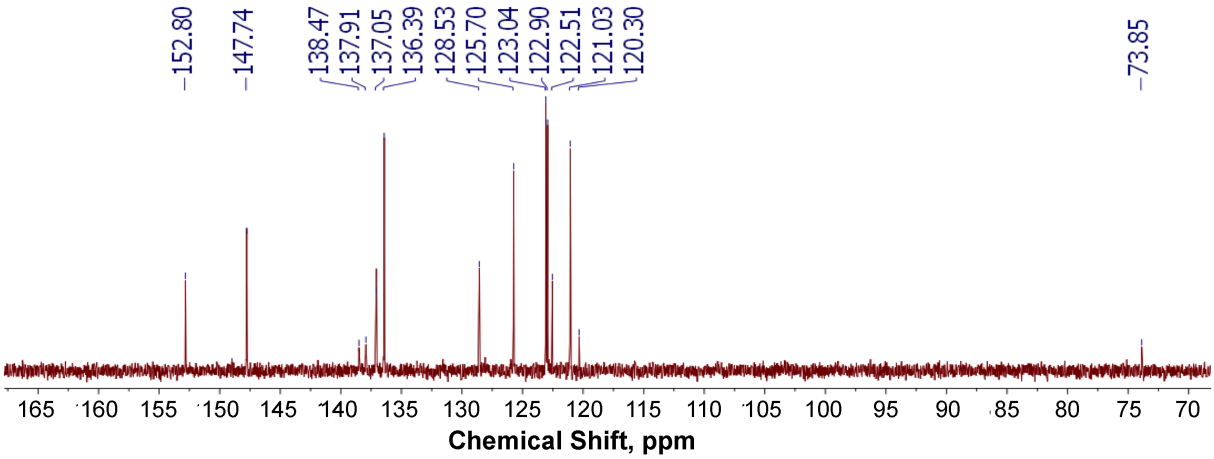

Figure S30. [13]C NMR of **L1**

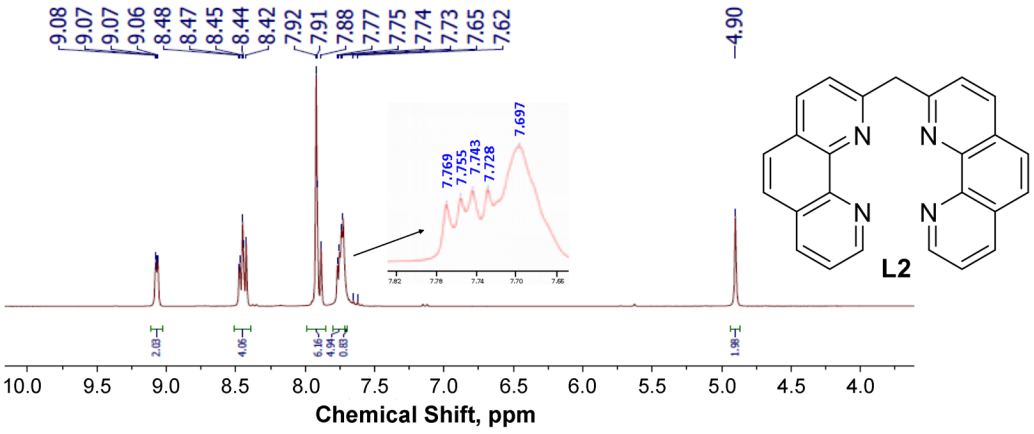

Figure S31. [1]H NMR of **L2**

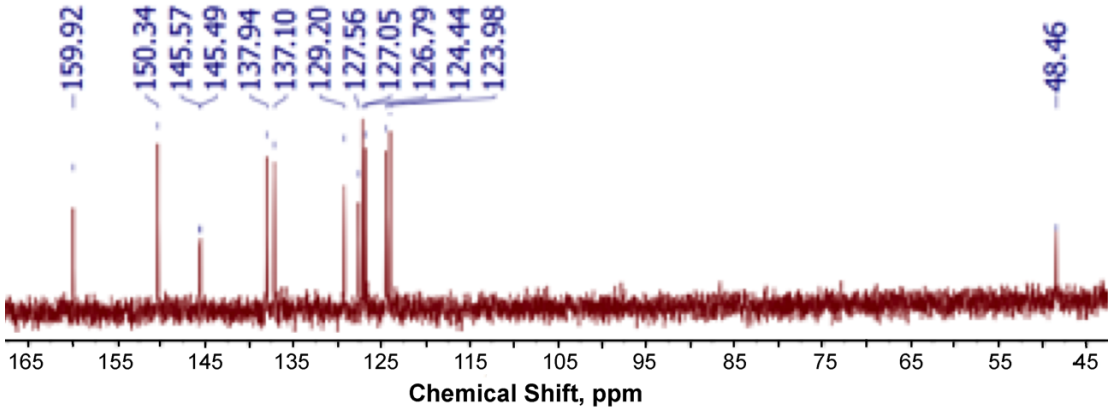

Figure S32. ^{13}C NMR of **L2**

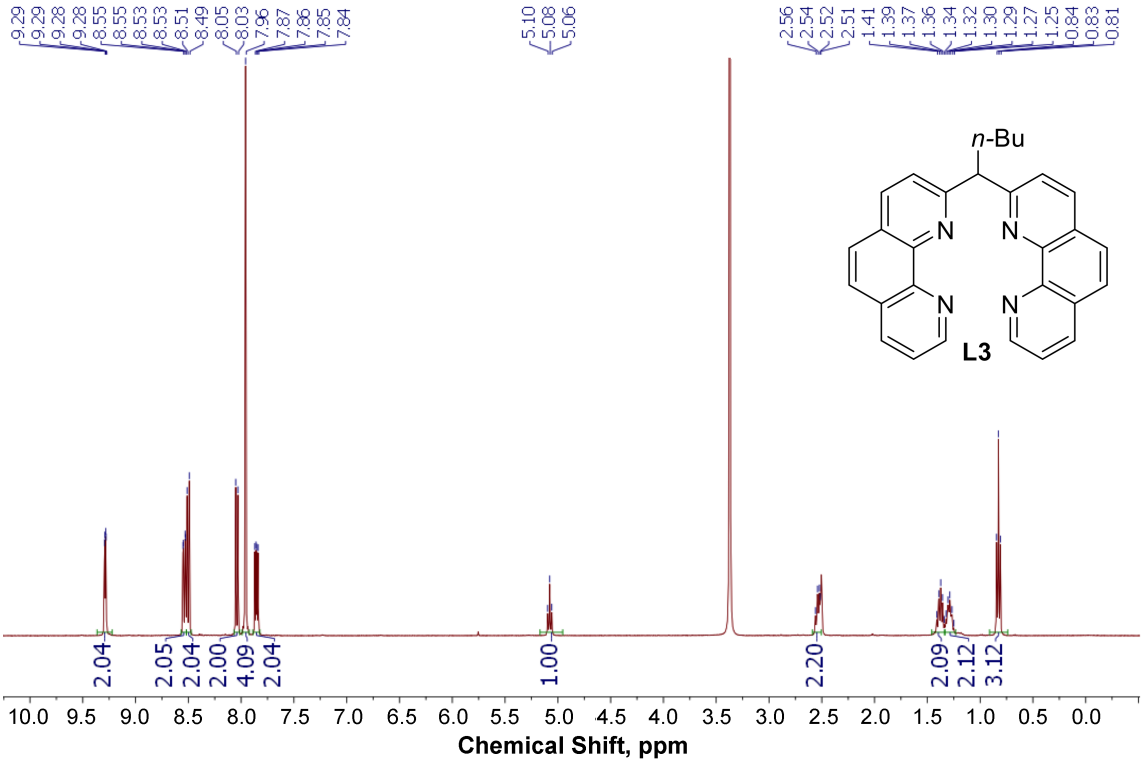

Figure **S33**. ^{1}H NMR of **L3**

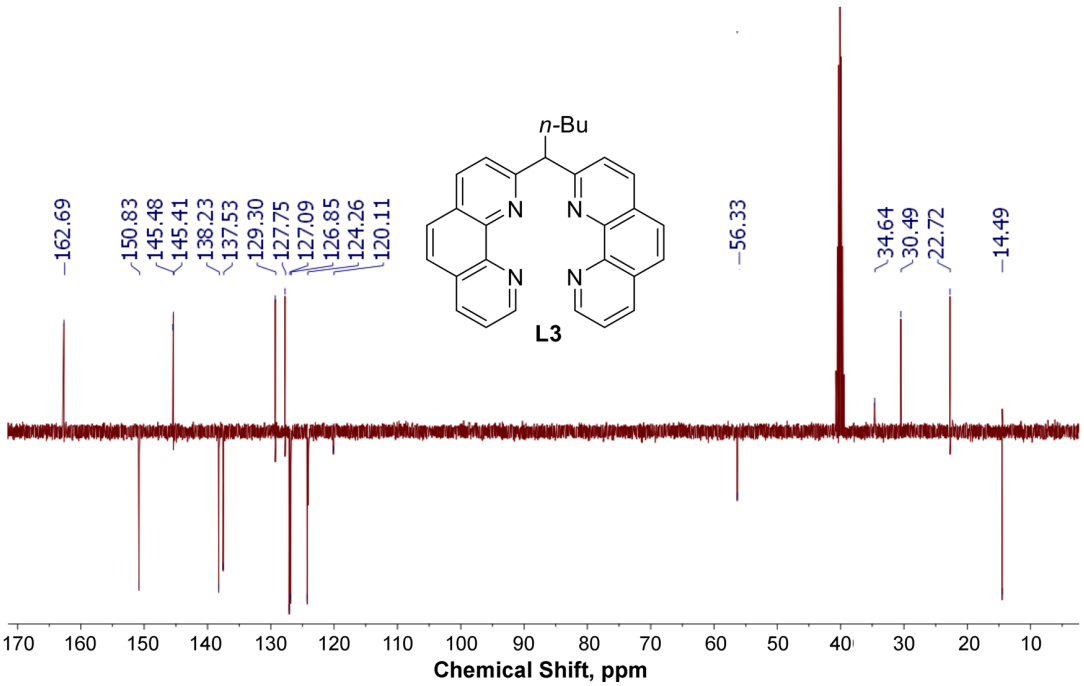

Figure S34. DEPT ^{13}C NMR of **L3**

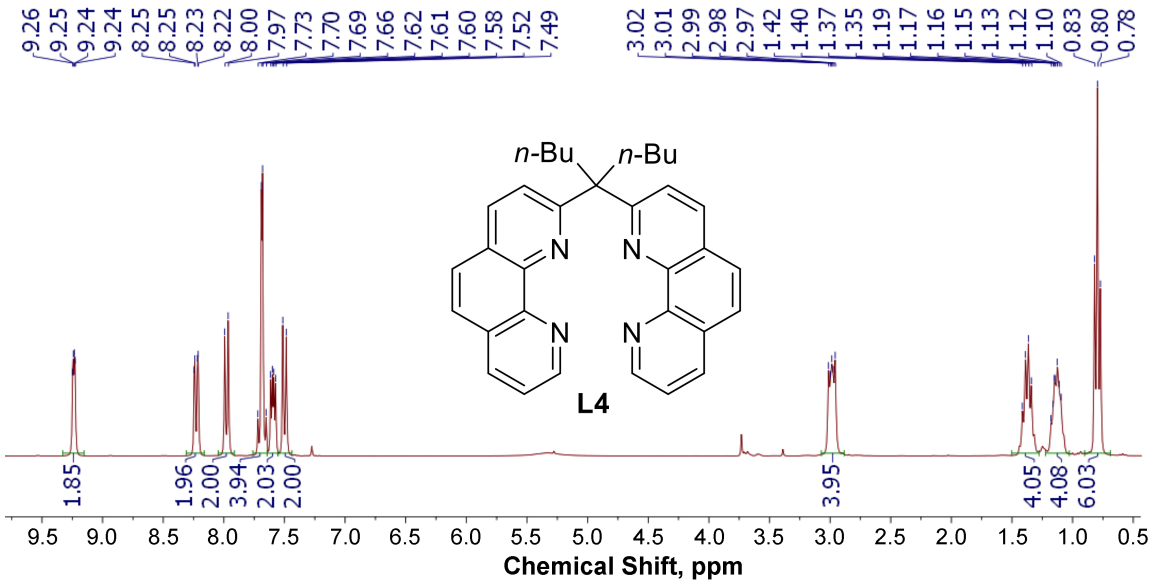

Figure S35. ^{1}H NMR of **L4**

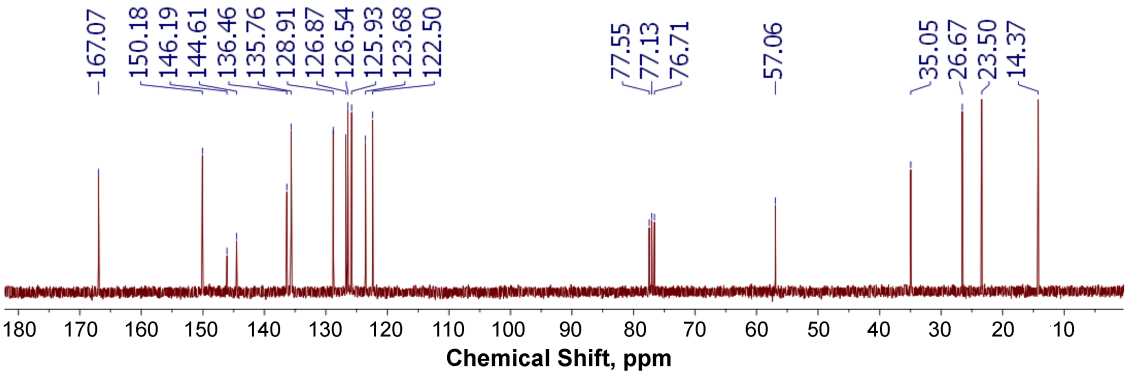

Figure S36. ^{13}C NMR of **L4**

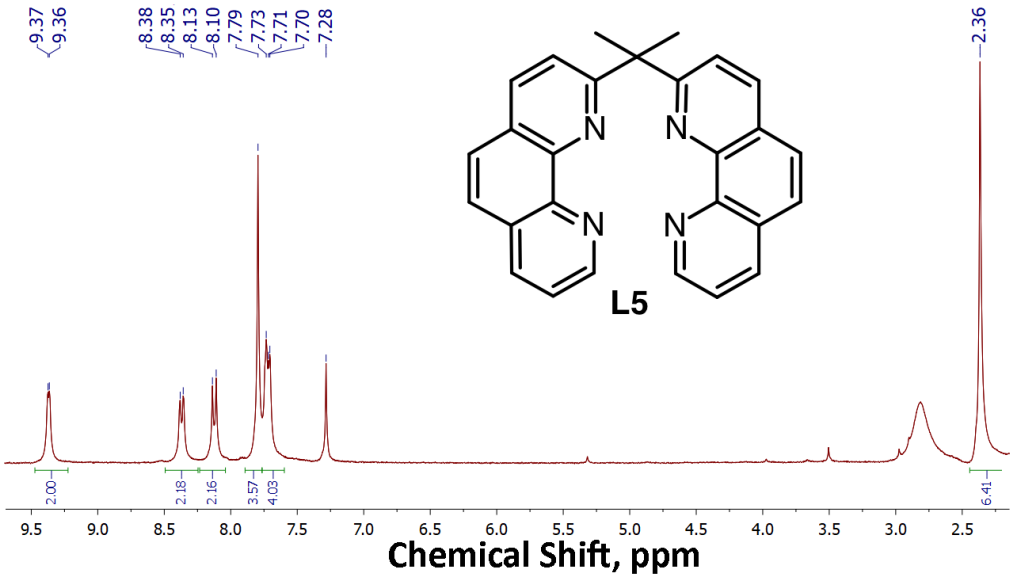

Figure S37. ^{1}H NMR of **L5**

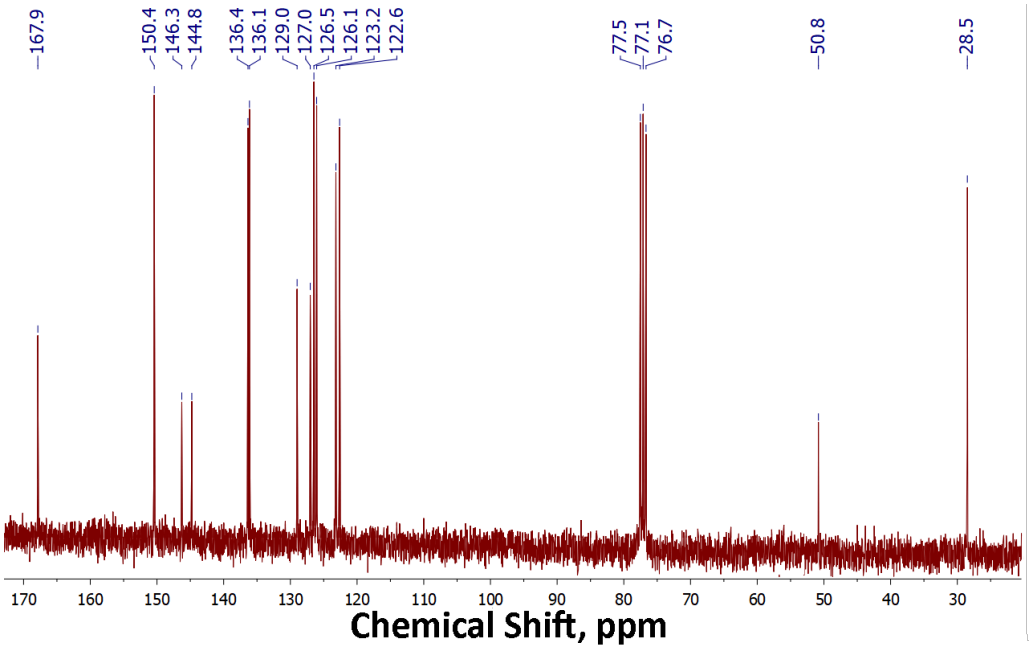

Figure S38. ^{13}C NMR of **L5**

Table S1. Crystal data and refinement parameters for complexes

Complex	**1**	**3**	**4**	**5**	**6**	**7**	**8**
CCDC number	1857319	1857316	1882739	1889967	1857313	1857315	1857317
Formula	$C_{29}H_{28}CoN_4O_2$, $2(PF_6)$, H_2O, C_2H_3N	$C_{31}H_{27}CuN_5$,$2(F_6P)$	$C_{33}H_{30}FeN_6$, $2(F_6P)$	$C_{58}H_{49}N_8OZn$, $3(C_2H_3N)$, $3(F_6P)$	$C_{33}H_{34}CoN_4O_2$, $2(F_6P)$, CH_4O	$C_{35}H_{37}N_5NiO$, $2(F_6P)$, $2(H_2O)$	$C_{66}H_{64}Cu_2F_{12}N_8P_2$, $2(F_6P)$, $2(C_2H_3N)$ [+ solvent]
Fw	872.49	823.05	856.42	1562.86	899.55	928.38	879.16
Crystal system	triclinic	monoclinic	monoclinic	triclinic	monoclinic	monoclinic	monoclinic
Space group	P-1	$P2_1/c$	P 21/c	P-1	$P2_1/c$	$P2_1/c$	$P2_1/c$
a(Å)	9.6288(2)	14.5775(1)	13.4587(10)	13.266(5)	20.5794(15)	8.90691(18)	12.4834(8)
b(Å)	12.0061(2)	13.1921(1)	12.5513(9)	16.158(6)	11.4538(7)	19.3126(4)	28.3893(16)
c(Å)	16.9177(2)	16.6972(1)	20.0189(14)	16.489(6)	18.0531(5)	23.1855(4)	20.6218(12)
α (deg)	100.669(1)	90(-)	90(-)	93.441(14)	90(-)	90(-)	90(-)
β (deg)	97.557(1)	98.116(1)	96.006(4)	103.769(13)	111.791(9)	99.2505(16)	98.475(6)
γ (deg)	111.039(1)	90(-)	90(-)	109.242(13)	90(-)	90(-)	90(-)
V($Å^3$)	1751.54(5)	3178.84(4)	3363.1(4)	3204(2)	3951.3(5)	3936.41(13)	7228.5(8)
Z	2	4	4	2	4	4	4
D_{calc} (g/cm^3)	1.654	1.720	1.691	1.620	1.512	1.567	1.616
μ (mm^{-1})	5.677	2.878	0.647	0.930	0.611	2.383	0.790
λ(Å)	1.54184	1.54184	0.71073	0.71073	0.71073	1.54184	0.71073
Data with I>2σ(I) Parameters	6357 519	6376 462	3728 536	15271 994	5290 528	6712 581	10521 1035
GOF on F^2	1.038	1.107	1.042	1.027	1.036	1.050	1.058
R1[a] wR2 [b]	0.0473 0.1285	0.0484 0.1386	0.0850 0.2021	0.0488 0.1248	0.0861 0.2431	0.0727 0.2056	0.0725 0.1691

[a] $R1=\Sigma||F_o|-|F_d||/\Sigma|F_o|$, [b] $wR2=[\Sigma w(F_o^2 - F_c^2)^2 / \Sigma w(F_o^2)^2]^1$

Table S1. Continuation

Complex	**9**	**10**	**11**	**12**	**13**	**16**	Fe-O-Fe dimer
CCDC number	1882738	1889966	1857314	1882740	1882741	1857318	1882737
Formula	$C_{54}H_{40}Fe_2N_8O_4S$, 2(F_6P), C_2H_3N	$C_{33}H_{32}ClN_4Zn$, F_6P, C_2H_3N	$C_{58}H_{46}Co_2N_8O_2$, 2(F_6P), 2(C_2H_3N)	$C_{58}H_{46}Fe_2N_8O_2$, 2(F_6P) [+solvent]	$C_{58}H_{46}Fe_2N_8O_2$, 3(F_6P), 2.758(CH_4O)	$C_{25}H_{16}CuN_4O_2$, 2(F_6P)	$C_{54}H_{40}Fe_2N_8O_9S_2$, 14($H_2O$)
Fw	1339.69	771.47	1376.93	1288.67	1522.07	757.90	1372.98
Crystal system	triclinic	triclinic	triclinic	triclinic	triclinic	monoclinic	monoclinic
Space group	P-1	P-1	P-1	P-1	P-1	$P2_1/n$	I 2/m
a(Å)	13.5658(1)	9.0269(2)	9.4342(2)	9.4135(3)	9.6742(19)	11.6270(1)	13.8024(4)
b(Å)	14.0483(1)	14.0229(4)	12.4800(3)	12.4551(4)	13.311(3)	14.4780(1)	15.8143(4)
c(Å)	14.1414(1)	15.4725(3)	12.6695(2)	12.8728(5)	13.419(3)	16.6429(2)	14.0624(3)
α (deg)	83.802(1)	114.122(2)	102.318(2)	103.555(2)	67.90(3)	90(-)	90(-)
β (deg)	84.964(1)	92.3850(10)	97.292(2)	97.785(2)	78.59(3)	109.253(1)	110.939(3)
γ (deg)	82.540(1)	105.600(2)	92.148(2)	92.746(2)	89.36(3)	90(-)	90(-)
V($Å^3$)	2649.14(3)	1695.92(8)	1442.35(5)	1448.74(9)	1565.7(6)	2644.91(5)	2866.77(14)
Z	2	2	1	1	1	4	2
D_{calc} (g/cm^3)	1.679	1.511	1.585	1.477	1.614	1.903	1.591
μ (mm^{-1})	6.232	2.763	5.857	0.644	5.425	3.443	5.526
λ(Å)	1.54184	1.54184	1.54184	0.71073	1.54184	1.54184	1.54184
Data with I>2σ(I)	10099	5391	5247	6649	5490	4926	2921
Parameters	780	445	408	398	498	416	228
GOF on F^2	1.043	1.245	1.074	1.053	1.177	1.025	1.068
R1[a]	0.0261	0.0796	0.0532	0.0444	0.0426	0.0390	0.0628
wR2 [b]	0.0706	0.2575	0.1526	0.1120	0.1233	0.1118	0.1508

[a] $R1=\Sigma||F_o|-|F_d||/\Sigma|F_o|$, [b] $wR2=[\Sigma w(F_o^2 - F_c^2)^2 / \Sigma w(F_o^2)^2]^{1/2}$